MDPI

Article

Geopolymeric Composites Containing Industrial Waste Reinforced with *Arundo donax* Fibers

Stefania Manzi * , Luisa Molari, Maria Chiara Bignozzi , Giulia Masi and Andrea Saccani

Department of Civil, Chemical, Environmental and Materials Engineering, University of Bologna, Via Terracini 28, 40131 Bologna, Italy; luisa.molari@unibo.it (L.M.); maria.bignozzi@unibo.it (M.C.B.); giulia.masi5@unibo.it (G.M.); andrea.saccani@unibo.it (A.S.)
* Correspondence: stefania.manzi4@unibo.it; Tel.: +39-051-209-0329

Abstract: Traditional Portland cement-based composites have a great environmental impact. Alkali-activated binders can offer an alternative, particularly if they can be obtained even partially from waste. Two residuals derived from the finishing steps of the traditional ceramic industry have been used as possible polymerizable sources mixed with metakaolin. Moreover, to contrast the low dimensional stability of alkali-activated materials and their mechanical brittleness, natural fibers derived from the *Arundo donax* plant have been added to the mortars. The use of renewable natural fibers instead of synthetic ones can contribute a further environmental advantage. The fresh (consistency) and cured (mechanical) properties of composite materials prepared with residuals and metakaolin were analyzed here. For comparison's sake, a reference set of composite materials not loaded with fibers but with an identical binder/sand and liquid/binder ratio was cast. A room-temperature curing condition was selected that, although inadequate to promote the short-time reactivity of the wastes, has a minimal energy requirement and allows on-site applications. A small-scale decrease in the properties in the compression mode tests was observed in the waste-modified mortars, while the *Arundo* addition improved their flexural strength and dimensional stability.

Keywords: sustainable materials; alkali-activated mortars; tile-production residuals; *Arundo donax* fibers; mechanical characterization

1. Introduction

Nowadays, climate change is recognized as a universal emergency that goes beyond national borders. Environmental awareness concerning the necessity to eliminate the use of non-renewable resources and the possibility of recycling different types of waste has widened the search for alternative materials in the building industry.

Portland cement-derived mortars and concretes are considered as high impact materials from an environmental point of view, on account of the huge carbon dioxide footprint involved in the production of the binder. The cement industry, indeed, generates about 7% of global CO_2 emissions through the calcination of limestone, burning fossil fuels to produce thermal energy, transportation and energy usage [1–3]. Mitigating strategies are presently being studied, trying to reduce to an as low as possible fraction the clinker used to formulate the final binder [4]. It is, however, rather difficult to go below a certain clinker fraction [5].

A different strategy concerns the use of completely alternative materials. Alkali-activated materials or geopolymers can be considered valuable candidates for the substitution [6,7], in that they are derived from industrial or anthropogenic wastes [8–11] and they can be activated at room temperature, in the same way as the traditional mortars/concretes. Some wastes have been intensively studied, such as fly ash, blast furnace slags, bottom ash, silica fume or red mud. Some concerns have, however, been expressed on the present and future overall availability of these resources, since the amount of material employed worldwide in the construction industry is huge and continually increasing. Accordingly,

the search for other possible sources of activable wastes is an important topic. The required characteristics for an eligible waste to be employed in geopolymerization are its amorphous nature and its content of silica and alumina and possibly a low dimension. Therefore, glass waste, construction and demolition waste (i.e., concrete, bricks) and even the residuals of organic matter combustion such as rice husk ash or peat soil palm oil fuel ash (POFA) [12] have been selected to produce alkali-activated binders.

In the present study, the possibility of exploiting the by-products of the tile industry derived from the finishing steps of production, that is, the glaze lapping powders of porcelain stoneware and the porcelain stoneware grinding powder, as partial substitutes of metakaolin in the formulation of a multiphase binder have been analyzed. In the north of Italy, a rough estimation accounts for an overall production of 70,000 tons/year of these wastes [13]. According to their composition and microstructure, these wastes could become reactive in alkaline conditions since they are mainly composed of silica and aluminum oxide. Moreover, they do not necessitate any grinding process as they already have a small dimension, suitable to be used as received and to be activated at low temperatures.

Although they are more environmentally sustainable and able to develop good mechanical properties in shorter times than the traditional Portland cement-based composites, geopolymers suffer from extreme brittleness and low dimensional stability. To overcome these drawbacks and increase their toughness and flexural strength, they can be modified by adding fibers like steel, polyvinyl alcohol (PVA), polyethylene (PE), polypropylene (PP), glass or basalt [14–19]. Recently, attention has been focused on natural [20–29], virgin [30] or recycled [31] carbon fibers. Natural fibers are renewable, low-cost and low-energy demanding materials with low density and interesting mechanical properties. They may suffer from some drawbacks related to the incomplete reproducibility of the previously cited mechanical properties deriving from the different environmental conditions that the plant may face during its growth. Moreover, natural fibers can be porous, hydrophilic and their surface can be covered by uncoherent, waxy matter that can compromise fiber–matrix adhesion. Nevertheless, a chemical or thermal pretreatment can largely reduce these drawbacks. One of the possible sources of natural fibers is grass plants and reeds in particular [32,33].

In the present research, small-length *Arundo donax* fibers randomly dispersed were used to modify metakaolin mortars containing the two different wastes previously described (i.e., glaze lapping powders from porcelain stoneware production and porcelain stoneware grinding powder). *Arundo* is a fast-growing plant, largely available in the Mediterranean region [34]. As to its chemical composition, *Arundo* has a high amount of cellulose (about 70 wt%) and a low amount of hemicellulose (about 15 wt%). Consequently, it shows good mechanical properties (elastic modulus of about 40 GPa [35]) provided by the cellulose fraction, even if lower than those of some species of *bamboo*, and a reduced hydrophilicity on account of the reduced hemicellulose content. So far, *Arundo* has been employed in the formulation of polymer matrix composites (both thermosetting, i.e., epoxy, polyester and thermoplastics such as PE, PP and polylactic acid (PLA)) [34,36–39] but its use in inorganic matrix has still to be thoroughly investigated.

2. Materials and Experimental Procedures

2.1. Materials

2.1.1. Wastes

Glaze lapping powders from porcelain stoneware production, hereafter defined as LP (around 20,000 tons/year), and porcelain stoneware grinding powder, hereafter defined as GP (around 50,000 tons/year), from Sassuolo/Fiorano (Italy) industrial district were used. Table 1 shows their chemical composition obtained by inductively coupled plasma optical emission spectrometry (ICP, ICP-OES Serie Optima 3200 XL, PerkinElmer (Waltham, MA, USA)) while Table 2 shows their size and density. The size was determined by laser granulometry (Malvern Mastersize 3000, Worcestershire, UK) while the density was obtained by water pycnometry (ISOLAB, Laborgerate GmbH, Eschau, Germany). GP

powders had almost the same composition as the studied metakaolin, while LP showed a lower amount of silica and a higher amount of calcium oxide. Both wastes had a higher content of alkaline oxides than metakaolin. Figure 1a shows the X-ray diffraction pattern (investigated by a PANalytical Empyrean diffractometer with copper anode material, detector PIXcel1D, Almelo, The Netherlands) of metakaolin while Figure 1b shows those of both wastes. The presence of an amorphous fraction, which plays a fundamental role in alkaline activation, is evident in both the powders from the hump present at low theta values ($15° < 2θ < 35°$). Crystalline phases such as quartz and mullite are also present, particularly in GP waste, while in LP alumina and calcium carbonate diffraction peaks are present but their intensity is extremely low.
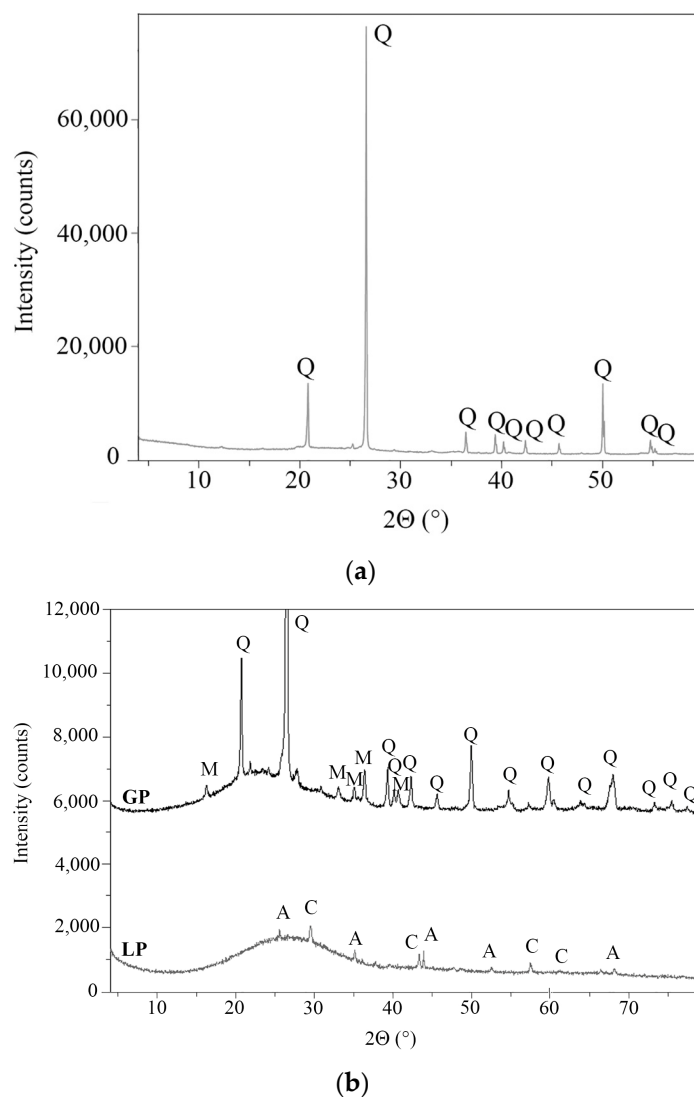

(a)

(b)

Figure 1. X-ray analysis: (**a**) metakaolin (Q = quartz); (**b**) selected LP and GP wastes (A = alumina, C = calcium carbonate, M = mullite, Q = quartz).

Table 1. Chemical composition (wt%) of metakaolin (MTK) and selected wastes (GP and LP).

Oxide	SiO_2	Al_2O_3	CaO	MgO	TiO_2	K_2O	Na_2O	LOI
MTK	72.0	22.1	0.4	0.1	1.0	0.3	0.04	2.4
GP	73.2	17.5	1.5	0.5	0.8	1.9	2.9	0.4
LP	53.5	15.2	11.7	1.1	0.1	3.9	4.7	6.2

Table 2. Size dimension (μm) and density (g/cm^3) of metakaolin (MTK) and selected wastes (GP and LP).

Sample	D$_{10}$	D$_{50}$	D$_{90}$	Density
MTK	106	43	5	2.50 $\pm$ 0.02
GP	89	22	4	2.46 $\pm$ 0.01
LP	20	5	2	2.43 $\pm$ 0.02

2.1.2. Binder

Flash calcined metakaolin, hereafter defined as MTK (ARGECO Development, Toulouse, France), was used as the main component of the matrix. It is derived from a low-energy process that minimizes the energy request. The powder dimension (determined by laser granulometry, Malvern Mastersize 3000, Worcestershire, UK) is reported in Table 2, as well as its density (obtained by water pycnometry, ISOLAB, Laborgerate GmbH, Eschau, Germany).

2.1.3. Aggregates

As aggregates, natural silica sand with a fixed grain size distribution (d$_{max}$ = 2 mm; SiO$_2$ > 96 wt%) was employed according to EN 196-1 Standard [40].

2.1.4. Fibers

Arundo donax fibers, 5 $\pm$ 1 mm long (Figure 2), were derived from the culms by mechanical methods (36 h in a NaOH 0.1 M solution, then a compression molding technique was used at 20 kN) partially following previous studies [41], and finally treatment with NaOH 1M solution for 2 h to remove waxy material and washing with distilled water. The density of the fiber measured by water pycnometry (ISOLAB, Laborgerate GmbH, Eschau, Germany) was 1.50 $\pm$ 0.08 g/cm^3.

Figure 2. Image of *Arundo donax* fibers.

2.1.5. Activators

As activators, a Na$_2$SiO$_3$ (SS, Ingessil, Verona, Italy) solution (ρ = 1.53 g/cm^3; SiO$_2$/Na$_2$O ratio = 2.07) and an 8 M molar solution of NaOH (Merck, Darmstadt, Germany) were employed in a 1:1 ratio.

2.2. Mix Design and Sample Preparation

First of all, the two alkaline activators were put together and left to cool down to room temperature. Then, metakaolin and GP or LP were added to the activators and blended with water in a Hobart mixer. Natural silica sand was included after 6 min. Finally, as the last component, *Arundo donax* fibers were added and mixed. In line with a previous

investigation [22], in the final matrix the proportion between MTK, activators, and H_2O was regulated to obtain a liquid/solid ratio of 0.48 and SiO_2/Al_2O_3 and Na_2O/SiO_2 ratios of 3.60 and 0.22, respectively. The liquid/solid ratio, as well as the ratio and amount of activators (NaOH and silicate), was kept constant in the mortars containing both wastes. In all the mortar mixes, the volume of *Arundo* was around 1.4%. In all the samples, the aggregate/binder ratio was 1:1, and the water/binder ratio was 0.13. Table 3 shows the composition of the investigated binders as well as the amount of fibers and the tags that were used afterwards in the text to identify them. Various samples were cast from the fresh composite materials: (a) $40 \times 40 \times 160$ mm prismatic specimens for mechanical and physical characterization; (b) cylindrical specimens (diameter = 35 mm, height = 100 mm) for water absorption by capillary and durability investigations; and (c) $25 \times 25 \times 280$ mm prismatic specimens for dimensional stability analysis.

Table 3. Mortar binder and fiber composition (grams) and mortar tags.

Sample	MTK	GP	LP	Fibers
MTK	100	0	0	0
MTK AR	100	0	0	3
MTK GP	85	15	0	0
MTK GP AR	85	15	0	3
MTK LP	85	0	15	0
MTK LP AR	85	0	15	3

2.3. Methods

2.3.1. Consistency

Following EN 1015-3 Standard [42], immediately after the procedure of mixing, the composite materials were cast in a truncated conical mold with a circular base (bottom diameter = 100 mm, top diameter = 70 mm, height = 60 mm). Finally, after the mold was removed and shaken, two perpendicular diameters of the collapsed mortar were measured, and the standard consistency (C) was thus determined following Equation (1)

$$C = 100 \cdot (d_m - d_0)/d_0, \tag{1}$$

where d_m is the average diameter of the two perpendicular diameters and d_0 is the lower diameter of the mold (i.e., 100 mm) (Figure 3).
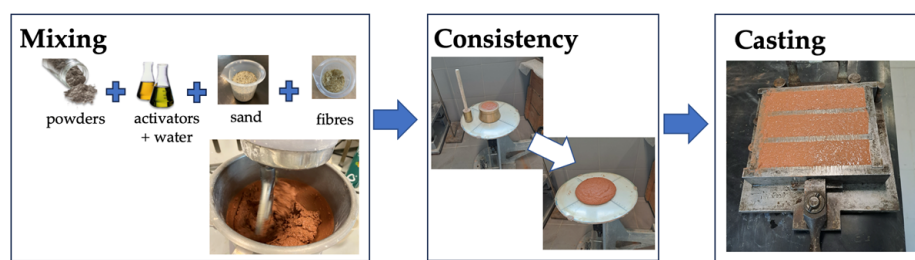

Figure 3. Mixing of composite materials, determination of consistency and casting of specimens for mechanical tests.

2.3.2. Physical Characterizations

The bulk density of the composite materials was obtained at 28 curing days following the EN 772-13 Standard [43].

2.3.3. Mechanical Characterizations

Both three-point flexural strength and compressive strength investigations were performed at 20 ± 1 °C and 65 ± 10 RH% using a Wolpert 100 kN test machine (Wolpert, Neu Ulm, Germany) with a speed rate of 5 mm/min. At the end of 28 curing days at 22 ± 2 °C

in sealed plastic bags, in the flexural condition, at least 5 specimens were tested, while in the compressive condition, 8 specimens were tested. With the only exception of these specifications, the method complied with the recommendations of the EN 196-1 Standard for Portland cement composite materials.

The flexural strength was determined according to EN 196-1, following Equation (2)

$$R_f = (1.5 \cdot F_f \cdot l)/b^3, \tag{2}$$

where R_f is the flexural strength (MPa), b is the side of the square section of the prism (mm), and F_f is the load applied to the middle of the prisms at fracture (N).

The compressive strength was determined according to EN 196-1, following Equation (3)

$$R_c = F_c/A, \tag{3}$$

where R_c is the compressive strength (MPa), F_c is the maximum load at fracture (N), and A is the area (mm^2) of the platens or auxiliary plates (40 × 40 mm).

2.3.4. X-ray Diffraction Analysis

To investigate the mineralogical composition of the composite materials, XRD analysis was carried out. An Empyrean Malvern Panalytical diffractometer, with detector PIXcel1D equipped with Cu radiation operating at 40 kV and 20 mA, was used to obtain the diffraction patterns. Samples were previously pulverized and scanned between 0° and 90° 2θ.

2.3.5. Mercury Intrusion Porosimetry

In order to estimate qualitatively and quantitatively the open porosity of the mortars, samples were fractured after 28 days of curing and chunks, whose weights were about 1 g, were submitted to mercury intrusion porosimetry (MIP, Pascal 140 and 240 Mercury Porosimeters instruments (Thermo Fisher Scientific, Waltham, MA, USA). A contact angle value of 141° and a surface tension value of 0.48 N/m were used for mercury. Samples were degassed for 30 min and a vacuum condition of 0.03 KPa was reached. A maximum pressure value of 200 MPa was achieved in MIP equipment. Every evaluation was reiterated at least twice. The S.O.L.I.D. software (v3.0, SOLver of Intrusion Data, Thermo Fisher Scientific, Waltham, MA USA) was used to manage all the MIP determinations. Due to the small volume that can be tested in the instrument, as well as the low fiber content, fiber-modified sample results are too scattered and consequently unreliable. Only data referring to the unmodified fiber samples, i.e., MKT, MKT GP and MKT LP, are reported.

2.3.6. Microstructural Analysis

SEM XL20 scanning electron microscopy (FEI, Hillsboro, OR, USA) was used to investigate the microstructure on non-perturbed fractured specimens attained after the flexural tests. Quorum 150R ES (Quorum Technologies Ltd., Judges House, Lewes, UK) was used to metallize specimens under vacuum. Throughout all SEM measurements, an accelerating voltage of 20 kV was adopted.

2.3.7. Water Absorption

According to EN 15801 Standard [44], the water absorption by the capillary of the mortars was determined on 3 cylinders (diameter = 35 mm, height = 100 mm) after 28 days of curing at 22 ± 2 °C. To determine moisture absorption in the function of time, a balance (Model CP225D, Sartorius, Gottingen, Germany) was employed. Formula (4) was used to calculate the amount of water absorbed in this way.

$$Q_i = (m_i - m_0)/A, \tag{4}$$

where m_0 is the weight of the sample in dried conditions (kg), m_i is the weight of the sample at time t_i (kg), A is the absorption area in contact with water (m^2), and Q_i is the amount of absorbed water at time t_i (kg/m^2).

2.3.8. Dimensional Stability

Following the ASTM C1012/C1012M Standard [45], the dimensional stability performance was tested on 3 prismatic specimens ($25 \times 25 \times 280$ mm) cured at 45 ± 3 RH % and 22 ± 2 °C.

3. Results and Discussion

The physical characterization of the composite materials is summarized in Table 4. Consistent changes took place in the diameter of the collapsed composites (d_m) and the consistency (C) of the fresh mortars. GP and LP had opposite effects. On account of the smaller dimension, LP decreased the consistency of the mortars while GP, having dimensions closer to metakaolin, slightly increased the flow value of the mortar possibly on account of the initial inertness of the powders. As could be expected, also the addition of *Arundo donax* decreased the diameter of the collapsed composites and the consistency of the composites. The extent of this effect was the same in the three matrices. Nevertheless, it was possible to cast all the samples without creating undesired porosities in the final specimens. This observation is supported by the bulk density data reported in the same table. A slight decrease took place as both ceramic wastes and fibers were added. In the latter case, this could be predicted on account of the lower density of the organic phase. However, experimental values were quite close to the theoretical ones derived by the single-phase contribution in the fresh state (2.00 g/cm^3 for MTK), a feature that implies the absence of macrovoids in the specimens.

Table 4. Physical and consistency properties of composite materials.

Sample	Density (g/cm^3)	d_m (mm)	C (%)
MTK	2.01 ± 0.03	194 ± 8	94
MTK AR	2.00 ± 0.06	183 ± 10	83
MTK GP	1.97 ± 0.05	202 ± 6	102
MTK GP AR	1.95 ± 0.07	190 ± 9	90
MTK LP	1.98 ± 0.05	179 ± 7	79
MTK LP AR	1.97 ± 0.06	168 ± 9	68

d_m = average diameter measured during the standard consistency test; C = consistency.

The flexural and compressive strength of the composite materials (Figure 4) at 28 days of room temperature curing are displayed in Figure 5a,b, respectively. In all samples, the flexural strength was increased (about +18% on average) by the *Arundo* addition and the negative effect of the wastes was limited (about −3% for GP). Compared to other fibers, i.e., *Moso bamboo*, kenaf and hemp at almost the same relative volume amount [22], the strengthening effect on the metakaolin sample was close to that found for kenaf fibers and lower than the one obtained with *Moso bamboo*. The 18% increase in flexural strength agrees with other research (+15%) [46] but was lower than in [32] (about +30%), where, however, a higher fiber amount (5%wt) was used. As to the aspect of the fracture surface derived from the flexural tests, the presence of both waste and fibers did not alter the brittle morphology of the matrix failure. The fracture ran almost perpendicularly to the main axis of the tested specimens without the formation of multiple macrocracks and a pull-out process of the fibers was observed (Figure 4). A stronger negative effect was instead evident in compression mode. In GP mortar, the strength was 18% lower while a −10% was recorded for LP. Fiber addition had a negligible effect (−5% in the worst case, MTK) on this property which was much lower than what was found in other research [32].

Figure 4. Image of MTK GP AR specimens tested for mechanical properties at 28 days of curing.
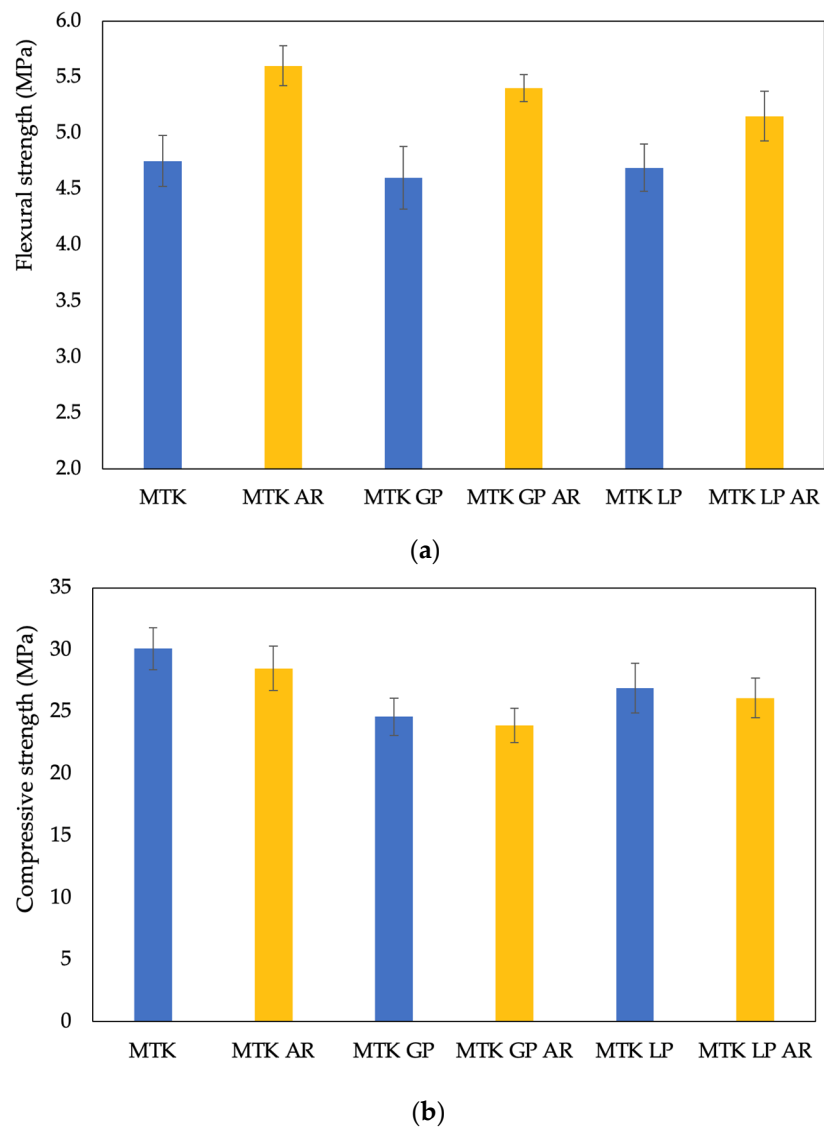

(**a**)

(**b**)

Figure 5. Mechanical characterizations at 28 days of curing: (**a**) flexural; (**b**) compressive strength.

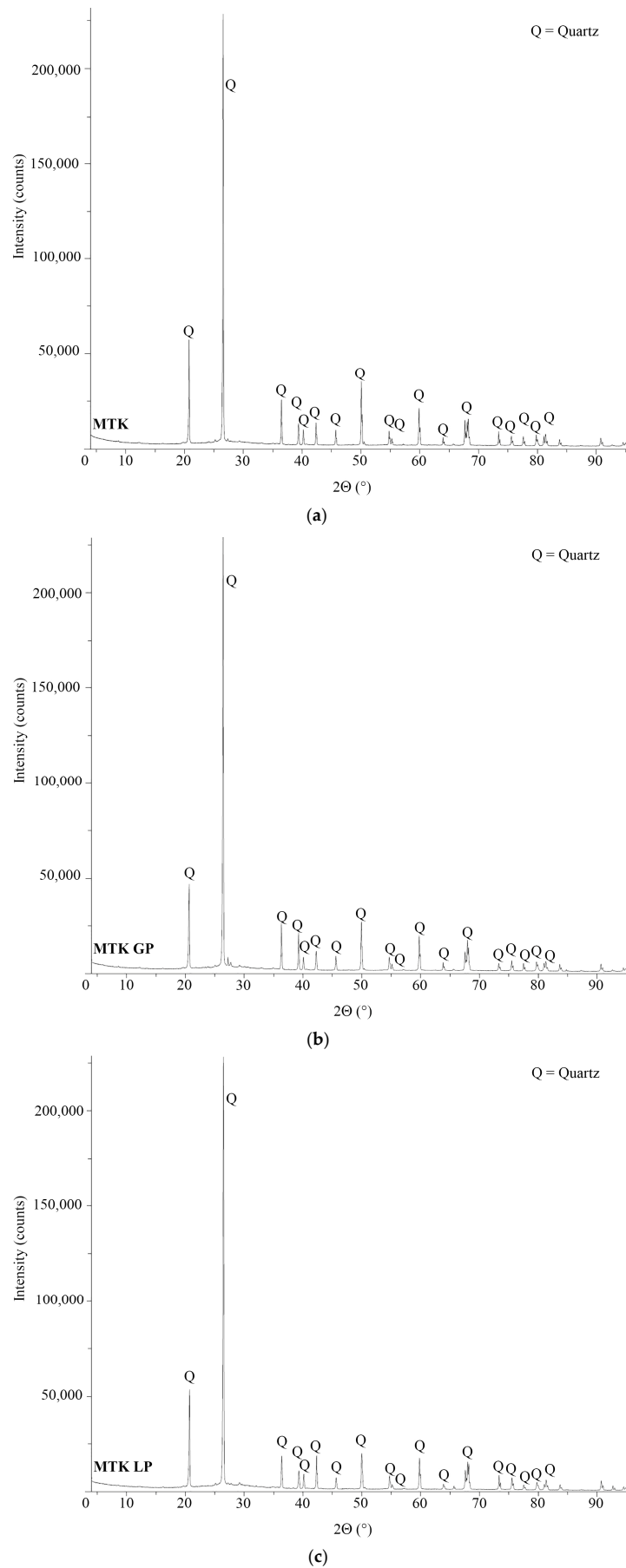The X-ray analysis of the three grounded mortars is shown in Figure 6.

Figure 6. X-ray analysis of the grounded mortars after 28 days of curing: (**a**) MTK; (**b**) MTK GP; (**c**) MTK LP.

The only peaks that appeared on the diffractogram were those of silica, while no other phases were recorded. The presence of silica is derived from the crystalline phase already present in metakaolin (Figure 1a) and, to a limited extent, from the smaller natural aggregate particles that could not be completely separated from the matrix. The disappearance of other phases previously detected in GP and LP derives both from their low amounts in the matrix but could also derive from a partial reactivity of these phases. At the same time, it is noteworthy to underline the absence of peaks related to sodium hydroxide and silicate in all samples. This feature implies that the activating reagents are involved in the formation of crosslinked structures, albeit with different compositions, even in the waste-modified mortars.

The results concerning the mercury intrusion porosimetry tests are summarized in Figure 7. As reported previously, they only refer to the samples without fibers.
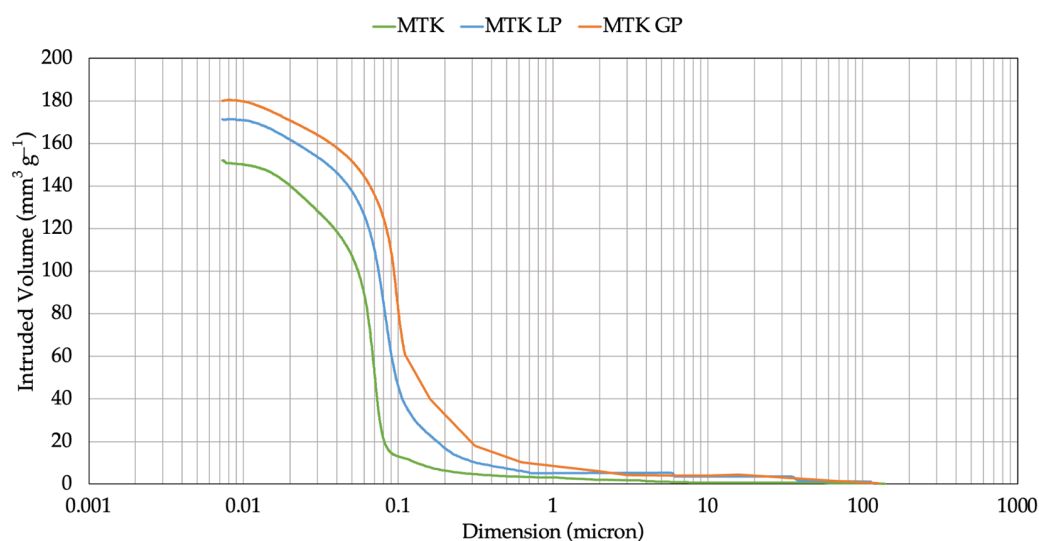
Figure 7. MIP results on the three investigated mortars without fibers after 28 days of curing.

The high dimension porosity fractions, that is, pores having a dimension above 1 μm, were relatively small. MTK had the lowest values but both LP and GP modified mortars did not exceed 10 mm³/g. This agrees with the density results that showed close values among the samples and close also to the theoretical ones. Substantial differences were instead found at lower dimensions (<1 μm). MTK has the lowest overall open porosity with an average pore size of about 0.05 μm. The LP powders increase both the overall open porosity and shift the average pore size to a value of about 0.07 μm. The same effect takes place with GP powders but with a further shift of the average pore size to about 0.1 μm. These results support the results of the mechanical tests (Figure 5): the higher porosities led to lower compressive strength in LP and, more consistently, in GP samples compared to the unmodified MTK samples.

The microstructure of the samples derived from the fractured surfaces after 28 days of curing is reported in Figure 8. All the matrices showed a compact morphology with well-dispersed GP and LP powders. A close examination revealed the presence of some unreacted GP particles with dimensions higher than 30 μm (see Figure 8d) which, on account of their close chemical composition, were well embedded in the metakaolin matrix. Figure 8e,f show the aspect of the *Arundo* fibers in the composites. Although no porosities are present at the interphase, their surface is smooth and uncovered by matrix residuals, a feature suggesting that a different surface treatment could further improve the flexural strength as performed with polymeric matrix [47,48].
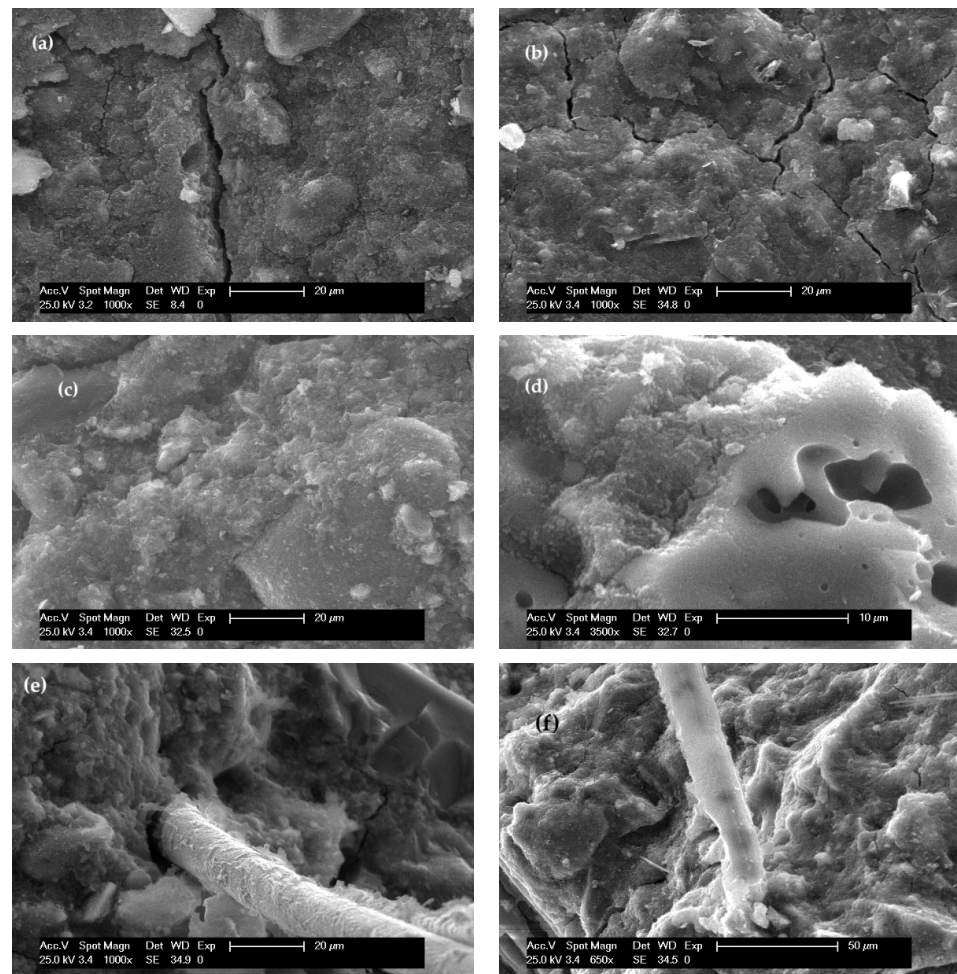
Figure 8. Morphology of the matrix (**a**) MTK, (**b**) MTK GP, (**c**) MTK LP; (**d**) unreacted particle in MTK GP samples; and *Arundo* fibers in (**e**) MTK AR and (**f**) MTK GP AR composites.

Water absorption by capillary test can be considered as a tool to predict the long-term durability of the mortars. A high rate of capillary absorption implies the faster diffusion of ions in the composite possibly leading to undesired chemical reactions. Figure 9 shows the effect of the addition of GP and LP to the metakaolin binder. While LP waste slightly increases the rate of absorption, GP waste has a more negative effect on the process. Figure 10 shows the experiments relative to the fiber-modified mortars. Two points can be underlined: (a) the presence of fibers does not increase the rate of absorption in all the samples. This means that no preferential paths are generated either by the fiber itself or by the fiber–matrix interphase, a feature that seems to support what is observed in Figure 8. (b) A decrease is instead observed in the rate of absorption, particularly for the MTK GP AR sample. A possible explanation is the substitution of a porous matrix fraction with the *Arundo donax* fiber, which is a less porous phase. The effect is thus more intense in the case of GP-modified paste that, also on account of the lower compressive strength (Figure 5), should have the highest porosity. In Table 5, the coefficients of capillary water absorption are reported.

Table 5. Coefficient of capillary water absorption ($kg/(m^2 s^{1/2})$) of the investigated mortars.

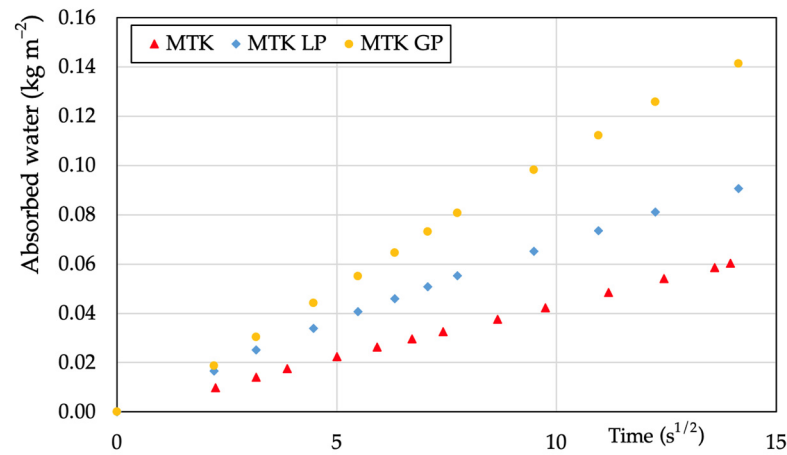| Binder	No Fibers	Fibers
MTK	4.2×10^{-3}	3.6×10^{-3}
MTK GP	10.3×10^{-3}	7.7×10^{-3}
MTK LP	6.3×10^{-3}	6.0×10^{-3}

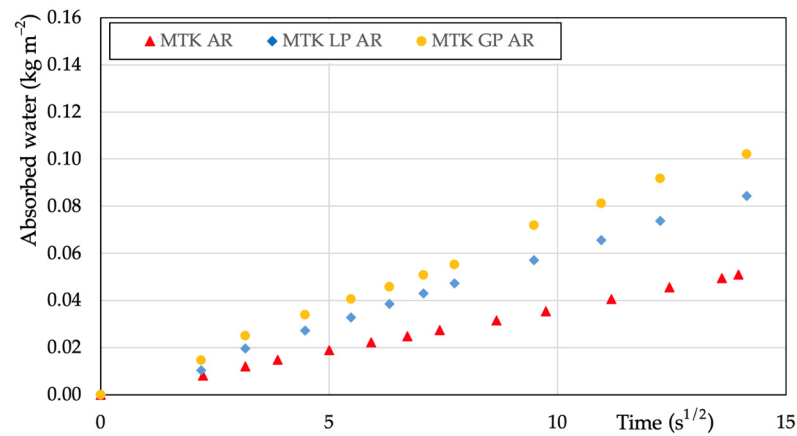**Figure 9.** Water absorption by capillarity of composite materials without fibers.

Figure 10. Water absorption by capillarity of composite materials modified by fibers.

Finally, Figure 11 shows the dimensional variation in the different samples after 14 days of curing. Waste additions have almost no influence on shrinkage, while *Arundo* fibers manage to increase the stability of the bare metakaolin mortar. The effect is comparable in pure metakaolin and waste-modified binders. The constraining effect of the fibers, increasing the dimensional stability of the composite, is usually dependent on the fiber–matrix interaction. In our case, the presence of waste, also on account of the low amounts, did not affect the friction between the two phases. This feature seems to support the observation derived from the previous experiment, that the increased porosity affects the bulk of the matrix and not the fiber–matrix interphase.
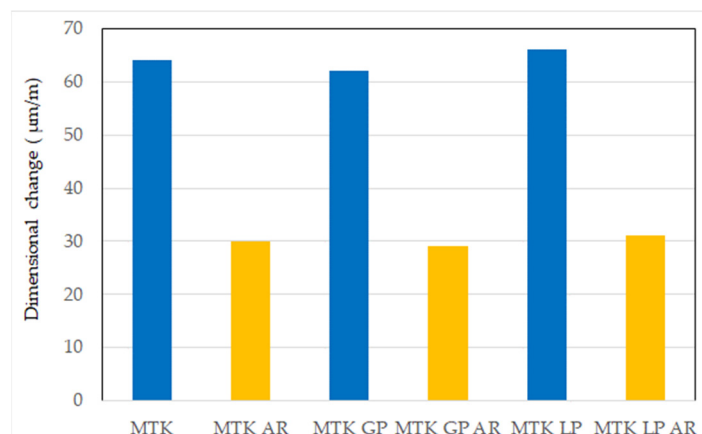

Figure 11. Dimensional variation between the different samples after 14 days of curing.

4. Conclusions

In the present research, an attempt to introduce industrial waste with potential reactivity to alkaline activators in an alkali-activated metakaolin matrix was performed. The main results can thus be summarized:

- A room temperature curing process was selected, a condition that does not promote the waste dissolution but on the contrary, would enable on-site application of the materials. Moreover, since the reactive fraction of the different wastes is unknown, the same activator amount and ratio was considered for the modified mortars, thus unavoidably leading to an unbalanced ratio among the different oxides (Na_2O/SiO_2 and Al_2O_3/SiO_2 ratios).
- X-ray analysis performed on the cured mortars, however, did not show the presence of unreacted activators. Therefore, it can be supposed that the presence of the waste alters the final composition of the reacted gels leading to less developed networks but it does not hinder their formation.
- At the investigated fraction, only a slight detrimental effect was recorded on the compressive strength that remained above 25 MPa, which would allow its use in structural repairs.
- A slight reduction in consistency was also recorded but the value still enabled us to cast specimens without macroscopical porosities as revealed from the density measurements and morphological investigations.
- LP, on account of the lower dimensions and higher amorphous character, provides higher mechanical properties hinting at a limited but effective reactivity. This is also reflected by the decrease in porosity derived by MIP as well as the decrease in water absorption by the capillary action of the mortar when compared to the GP-modified sample.
- The addition of *Arundo* managed to increase the flexural strength and the dimensional stability of the mortars, slightly affecting the compressive strength.
- A positive effect from the use of natural fibers was also found in the rate of water absorption.

A reliable quantitative evaluation of the effective reactivity of the wastes at higher temperatures, enabling the development of an optimized-mix design or a targeted treatment of the fibers, could lead to higher mechanical properties but would then suffer from environmental and logistical drawbacks. Indeed, in these conditions, it is possible to formulate materials with helpful properties in the simplest conditions that could be applied on-site.

References

1. Supriya; Chaudhury, R.; Sharma, U.; Thapliyal, P.C.; Singh, L.P. Low-CO_2 emission strategies to achieve net zero target in cement sector. *J. Clean. Prod.* **2023**, *417*, 137466. [CrossRef]
2. Antunes, M.; Santos, R.L.; Pereira, J.; Rocha, P.; Horta, R.B.; Colaço, R. Alternative clinker technologies for reducing carbon emissions in cement industry: A critical review. *Materials* **2022**, *15*, 209. [CrossRef] [PubMed]

3. Juenger, M.C.G.; Snellings, R.; Bernal, S.A. Supplementary cementitious materials: New sources, characterization, and performance insights. *Cem. Concr. Res.* **2019**, *122*, 257–273. [CrossRef]
4. Cuesta, A.; Ayuela, A.; Aranda, M.A.G. Belite cements and their activation. *Cem. Concr. Res.* **2021**, *140*, 106319. [CrossRef]
5. Miller, S.A. Supplementary cementitious materials to mitigate greenhouse gas emissions from concrete: Can there be too much of a good thing? *J. Clean. Prod.* **2018**, *178*, 587–598. [CrossRef]
6. Sofi, M.; van Deventer, J.S.J.; Mendis, P.A.; Lukey, G.C. Engineering properties of inorganic polymer concretes (IPCs). *Cem. Concr. Res.* **2007**, *37*, 251–257. [CrossRef]
7. Abulencia, A.B.; Villoria, M.B.D.; Libre, R.G.D.; Quiatchon, P.R.J.; Dollente, I.J.R.; Guades, E.J.; Promentilla, M.A.B.; Garciano, L.E.O.; Ongpeng, J.M.C. Geopolymers as sustainable material for strengthening and restoring unreinforced masonry structures: A review. *Buildings* **2021**, *11*, 532. [CrossRef]
8. Tahwia, A.M.; Abd Ellatief, M.; Heneigel, A.M.; Abd Elrahman, M. Characteristics of eco-friendly ultra-high-performance geopolymer concrete incorporating waste materials. *Ceram. Int.* **2022**, *48*, 19662–19674. [CrossRef]
9. Provis, J.L.; Palomo, A.; Shi, C. Advances in understanding alkali-activated materials. *Cem. Concr. Res.* **2015**, *78*, 110–115. [CrossRef]
10. Gu, F.; Xie, J.; Vuye, C.; Wu, Y.; Zhang, J. Synthesis of geopolymer using alkaline activation of building-related construction and demolition wastes. *J. Clean. Prod.* **2023**, *420*, 138335. [CrossRef]
11. Epure, C.; Munteanu, C.; Istrate, B.; Harja, M.; Buium, F. Applications of recycled and crushed glass (RCG) as a substitute for natural materials in various fields—A Review. *Materials* **2023**, *16*, 5957. [CrossRef] [PubMed]
12. Amaludin, A.E.; Asrah, H.; Mohamad, H.M.; bin Amaludin, H.Z.; bin Amaludin, N.A. Physicochemical and microstructural characterization of klias peat, lumadan pofa, and GGBFS for geopolymer based soil stabilization. *HighTech Innov. J.* **2023**, *4*, 327–348. [CrossRef]
13. ARPAE. Available online: https://www.arpae.it/ (accessed on 13 December 2023).
14. Farhan, K.Z.; Johari, M.A.M.; Demirboga, R. Impact of fiber reinforcements on properties of geopolymer composites: A review. *J. Build. Eng.* **2021**, *44*, 102628. [CrossRef]
15. Abbas, A.G.N.; Aziz, F.N.A.A.; Abdan, K.; Nasir, N.A.M.; Huseien, G.F. A state-of-the-art review on fibre-reinforced geopolymer composites. *Constr. Build. Mater.* **2022**, *330*, 127187. [CrossRef]
16. Ranjbar, N.; Zhang, M. Fiber-reiforced geopolymer composites: A review. *Cem. Concr. Comp.* **2020**, *107*, 103498. [CrossRef]
17. Zuaiter, M.; El-Hassan, H.; El-Maaddawy, T.; El-Ariss, B. Properties of Slag-Fly Ash Blended Geopolymer Concrete Reinforced with Hybrid Glass Fibers. *Buildings* **2020**, *12*, 1114. [CrossRef]
18. Zhang, Z.; Zou, P.; Wang, Y.; Zhang, X. Impact of Nano-CaCO$_3$ and PVA fiber on properties of fresh and hardened geopolymer mortar. *Buildings* **2023**, *13*, 1380. [CrossRef]
19. Ramesh, V.A.; Jarghouyeh, E.N.; Alraeeini, A.S.; Al-Fakih, A. Optimisation investigation and bond-slip behaviour of high strength pva-engineered geopolymer composite (egc) cured in ambient temperatures. *Buildings* **2023**, *13*, 3020. [CrossRef]
20. Korniejenko, K.; Łach, M.; Mikuła, J. The influence of short coir, glass and carbon fibers on the properties of composites with geopolymer matrix. *Materials* **2021**, *14*, 4599. [CrossRef]
21. Silva, G.; Kim, S.; Aguilar, R.; Nakamatsu, J. Natural fibers as reinforcement additives for geopolymers—A review of potential eco-friendly applications to the construction industry. *Sustain. Mater. Technol.* **2020**, *23*, e00132. [CrossRef]
22. Saccani, A.; Molari, L.; Totaro, G.; Manzi, S. Geopolymers reinforced with natural fibers: A comparison among different sources. *Appl. Sci.* **2021**, *11*, 11026. [CrossRef]
23. Wongsa, A.; Kunthawatwong, R.; Naenudon, S.; Sata, V.; Chindaprasirt, P. Natural fiber reinforced high calcium fly ash geopolymer mortar. *Constr. Build. Mater.* **2020**, *241*, 118143. [CrossRef]
24. Manzi, S.; Molari, L.; Totaro, G.; Saccani, A. Alkali-Activated Mortars Reinforced with *Arundo donax*: Properties and Durability to Environmental Stresses. *Materials* **2023**, *16*, 3898. [CrossRef] [PubMed]
25. Moujoud, Z.; Sair, S.; Ousaleh, H.A.; Ayouch, I.; Bouari, A.E.; Tanane, O. Geopolymer composites reinforced with natural Fibers: A review of recent advances in processing and properties. *Constr. Build. Mater.* **2023**, *388*, 131666. [CrossRef]
26. Aperador, W.; Bautista-Ruiz, J.; Sánchez-Molina, J. Geopolymers based on a mixture of steel slag and fly ash, activated with rice husks and reinforced with *Guadua angustifolia* fibers. *Sustainability* **2023**, *15*, 12404. [CrossRef]
27. Vailati, M.; Mercuri, M.; Angiolilli, M.; Gregori, A. Natural-fibrous lime-based mortar for the rapid retrofitting of heritage masonry buildings. *Fibers* **2021**, *9*, 68. [CrossRef]
28. Angiolilli, M.; Gregori, A.; Cattari, S. Performance of fiber reinforced mortar coating for irregular stone masonry: Experimental and analytical investigations. *Constr. Build. Mater.* **2021**, *294*, 123508. [CrossRef]
29. Haily, E.; Zari, N.; Bouhfid, R.; Qaiss, A. Natural fibers as an alternative to synthetic fibers in the reinforcement of phosphate sludge-based geopolymer mortar. *J. Build. Eng.* **2023**, *67*, 105947. [CrossRef]
30. Zhang, D.; Wang, Y.; Zhang, T.; Yang, Q. Engineering and microstructural properties of carbon-fiber-reinforced fly-ash-based geopolymer composites. *J. Build. Eng.* **2023**, *79*, 107883. [CrossRef]
31. Manzi, S.; Lancellotti, I.; Masi, G.; Saccani, A. Alkali-Activated binders from waste incinerator bottom ashes and metakaolin reinforced by recycled carbon fiber composites. *Front. Mater.* **2020**, *7*, 583. [CrossRef]
32. Sá Ribeiro, R.A.; Sá Ribeiro, M.G.; Sankar, K.; Kriven, W.M. Geopolymer-bamboo composite—A novel sustainable construction material. *Constr. Build. Mater.* **2016**, *123*, 501–507. [CrossRef]

33. Libre, R.G.D., Jr.; Leaño, J.L., Jr.; Lopez, L.F.; Cacanando, C.J.D.; Promentilla, M.A.B.; Maximino, J.; Ongpeng, C. Microstructure and mechanical performance of bamboo fiber reinforced mill-scale—Fly-ash based geopolymer mortars. *Clean. Chem. Eng.* **2023**, *6*, 100110. [CrossRef]

34. Suarez, L.; Barczewski, M.; Kosmela, P.; Marrero, M.D.; Ortega, Z. Giant Reed (*Arundo donax* L.) fiber extraction and characterization for its use in polymer composites. *J. Nat. Fibers* **2023**, *20*, 2131687. [CrossRef]

35. Molari, L.; Coppolino, F.S.; García, J.J. *Arundo donax*: A widespread plant with great potential as sustainable structural material. *Constr. Build. Mater.* **2021**, *268*, 121143. [CrossRef]

36. Manniello, C.; Cillis, G.; Statuto, D.; Di Pasquale, A.; Picuno, P. Concrete blocks reinforced with *Arundo donax* natural fibers with different aspect ratios for application in bioarchitecture. *Appl. Sci.* **2022**, *12*, 2167. [CrossRef]

37. Ferrandez-García, A.A.; Ortuño, T.G.; Ferrandez-Villena, M.; Ferrandez-Garcia, A.; Ferrandez-García, M.T. Evaluation of particleboards made from giant reed (*Arundo donax* L.) bonded with cement and potato starch. *Polymers* **2022**, *14*, 111. [CrossRef]

38. Ortega, Z.; Romero, F.; Paz, R.; Suarez, L.; Benítez, A.N.; Marrero, M.D. Valorization of invasive plants from macaronesia as filler materials in the production of natural fiber composites by rotational molding. *Polymers* **2021**, *13*, 2220. [CrossRef]

39. Fiore, V.; Scalici, T.; Valenza, A. Characterization of a new natural fiber from *Arundo donax* L. as potential reinforcement of polymer composites. *Carbohydr. Polym.* **2014**, *106*, 77–83. [CrossRef] [PubMed]

40. *EN 196-1*; Methods of Testing Cement—Part 1: Determination of Strength. European Committee for Standardization: Brussels, Belgium, 2016.

41. Deshpande, A.P.; Rao, M.B.; Rao, C.L. Extraction of bamboo fibers and their use as reinforcement in polymeric composites. *J. Appl. Polym. Sci.* **2000**, *76*, 83–92. [CrossRef]

42. *EN 1015-3*; Determination of Consistency of Fresh Mortars by Flow Table. European Committee for Standardization: Brussels, Belgium, 2007.

43. *EN 772-13*; Determination of Net and Gross Dry Density. European Committee for Standardization: Brussels, Belgium, 2002.

44. *EN 15801*; Conservation of Cultural Property—Test Methods—Determination of Water Absorption by Capillarity. European Committee for Standardization: Brussels, Belgium, 2009.

45. *ASTM C1012/C1012M*; Standard Test Method for Length Change of Hydraulic-Cement Mortars Exposed to a Sulfate Solution. ASTM International: West Conshohocken, PA, USA, 2018.

46. Guo, C.; Li, M.; Wang, S.; Zhang, S.; Li, Y.; Li, C. Alkali treatment of bamboo fibers improves the mechanical properties of me-takaolin geopolymer. *J. Dispers. Sci. Technol.* **2023**, *45*, 980–989. [CrossRef]

47. España, J.M.; Samper, M.D.; Fages, E.; Sánchez-Nácher, L.; Balart, R. Investigation of the effect of different silane coupling agents on mechanical performance of basalt fiber composite laminates with biobased epoxy matrices. *Polym. Compos.* **2013**, *34*, 376–381. [CrossRef]

48. Sabarinathan, P.; Rajkumar, K.; Annamalai, V.E.; Vishal, K. Characterization on chemical and mechanical properties of silane treated fish tail palm fibres. *Int. J. Biol. Macromol.* **2020**, *163*, 2457–2464. [CrossRef] [PubMed]